Supporting Information

Liquor ammonia mediated V(V) insertion in thin Co_3O_4 sheet for improved pseudocapacitor with high energy density and high specific capacitance value

Ramkrishna Sahoo[1], Anindita Roy[1], Soumen Dutta[1], Chaiti Ray[1], Teresa Aditya[1], Anjali Pal[2] and Tarasankar Pal*[1]

[1]Department of Chemistry Indian institute of Technology, Kharagpur, India, [2]Department of Civil Engineering Indian institute of Technology, Kharagpur, India

Email: tpal@chem.iitkgp.ernet.in

S 1. Experimental methods:

Synthesis of Co_3O_4 nanosheets (C_1): Large scale Co_3O_4 ultrathin nanosheet was prepared from co-precipitation method. First, 10 mL 0.05 M $CoSO_4$, $7H_2O$ aqueous solution was taken in 15 mL screw capped test tube. Then, 300 µL liquor ammonia solution was injected to the previous solution and shaken to make the mixture homogeneous. There after the system was tightly capped and kept in modified hydrothermal reaction condition at 180 °C. After 24 h the grey product was centrifuged and washed with distilled water and ethanol to remove all the inorganic impurities. Finally the product was dried in vacuum and stored.

Synthesis of $Co_3V_2O_8$ nanosheets (C_2): Large scale $Co_3V_2O_8$ ultrathin nanosheet was also prepared from a co-precipitation method. First, a mixture of 5 mL 0.05 M $CoSO_4$, $7H_2O$ and 5 mL 0.05 M $VOSO_4$ aqueous solution was prepared. Then the mixture was taken in a 15 mL screw capped test tube. An aliquot of 300 µL liquor ammonia solution was injected into the previous solution and shaken to make the reaction mixture homogeneous. After that the reaction mixture in the test tube was capped and subjected to modified hydrothermal reaction condition at 180 °C. After 24 h the grey product was centrifuged and washed with distilled water and ethanol to remove all the inorganic impurities. Finally the product was dried in vacuum and stored.

Powder X-ray diffraction (XRD) was performed with a BRUKER-AXS-D8-ADVANCE difractometer (Cu target). The XRD data analysis was carried out using JCPDS software. X-ray photoelectron spectroscopy (XPS) analysis was executed with VG Scientific ESCALAB MK II spectrometer equipped with a Mg Kα excitation source (1253.6 eV) and a five-channeltron detection system to analyse the oxidation state of the elements. Field emission scanning electron microscopy (FESEM) analysis was performed with a Supra 40 (Carl Zeiss Pvt. Ltd) instrument and EDAX machine (Oxford link and ISIS 300) attached to the instrument was used to carry out the compositional analysis of the nanocrystal. Transmission electron microscopic (TEM) analysis was done in a Hitachi H-9000 NAR instrument using an accelerating voltage of 300 kV. Scanning transmission electron microscopy (STEM) analysis was carried out using AURIGA compact

instrument. Atomic force microscopy (AFM) was performed using Agilent Technologies, model No – 5550 AFM, tapping mode, cantilever frequency-160 KHz, cantilever length – 100 μM, radius of curvature of tip – 10 nm, tip material – SiN.

Electrochemical measurements:

The electrochemical performance has been tested using three electrode system measurements at room temperature. A stock KOH solution (3 M) was used as the electrolyte. Electrochemical studies of both the as-synthesized products were carried out by cyclic voltammetry (CV), chronopotentiometry (CP) or galvanostatic charge-discharge (GCD) and electrochemical impedance spectroscopy (EIS) technique. During the analysis glassy carbon electrode, Pt wire and saturated calomel electrode (SCE) were used as the working, counter and reference electrode, respectively. 7 μL of 1 g/L aqueous dispersion of electrode material was drop casted on the glassy carbon electrode and 5 μL of 0.05 wt% ethanolic nafion solution was used as the binder. It was left for 12 h. Before starting the experiments electrodes are dipped in 3M KOH electrolyte for 15 min. All the electrochemical measurements were carried out using CHI 660E electrochemical workstation.

S.2. EIS analysis of the $Co_3V_2O_8$ and Co_3O_4 pseudocapacitor:

Figure S13a,b displays the Nyquist plot for C_1 and C_2 samples before and after the 10000 charge-discharge cycles and Figure S13c contains the corresponding equivalent circuit. EIS measurements have been done within the frequency range from 0.1 Hz to 10^5 Hz at AC voltage amplitude of 5 mV. Table S4 illustrates the calculated parameters obtained by fitting the Nyquist plot with the Randles equivalent circuit. R_S stands for the internal resistance which includes the internal resistance of the electrode, ionic resistance of the electrolyte and interfacial resistance between the electrode surface and electrode material. From Table S4 it is observed that after 10000 cycles, R_S value decreases for both C_1 and C_2. This may be due to interfacial detachment of the glassy carbon electrode and the material. R_{CF} stands for the charge-transfer resistance. In our case increase in R_{CF} for C_1 is much more than the C_2 after 10000 cycles. In case of C_2, the ultrathin structure remains almost intact but C_1 structure ruptures during charge-discharge process, at high current density. Thus, after 10000 cycles charge transportation remains almost the same for C_2. In the Nyquist plot (Figure S13), the quasi

vertical lines, leaning to the imaginary axis ($Z^{//}$) in the low frequency region, stand for the Warburg constant which designates the diffusive resistance. Table S4 illustrates the diffusive resistance of the C_1 and C_2 samples before and after the 10000 cycles. According to that initially diffusive resistance for C_1 is higher than C_2 and after 10000 charge-discharge cycles rate of increase of diffusive resistance for C_1 is greater than C_2.

S 3. Calculation details of the electrochemical analysis:

$$\text{Specific capacitance, } C_{sp} = \left(\int_{v1}^{v2} iVdv\right)/mv(V2 - V1) \quad \text{----------1}$$

Where, the numerator stands for the total charge, m for electrode mass, ν for the scan rate, and (V2 −V1) is for the potential window.

$$\text{Specific capacitance, } C = it/m\Delta V \text{ ---------- 2}$$

Where, i signifies the constant cathodic current, t signifies the discharge time, m the weight of the active mass and ΔV is the potential window.

$$\eta = t_D/t_C \times 100 \text{ ---------- 3}$$

t_D is the discharging time and t_C is the charging time.

$$\text{Energy density, } E = \tfrac{1}{2}C\Delta V^2 \text{ ---------- 4}$$

$$\text{Power density, } P = E/T \text{ ---------- 5}$$

Where, C denotes the specific capacitance at current density, ΔV is the potential window, and T is the discharge time.

S.4. Asymmetric Supercapacitor:

To design asymmetric supercapacitor here we have used Co_3O_4 (C_1) and $Co_3V_2O_8$ (C_2) as the positive electrode and activated carbon (AC) as the negative electrode. To fabricate positive electrode we have dispersed Co_3O_4 or $Co_3V_2O_8$, acetylene black and polyvinylidene fluoride (PVDF) in NMP solvent in the weight ratio of 85:10:5. For the negative electrode we have dispersed AC, acetylene black and

PVDF in NMP solvent in the weight percentage of 85:10:5. Then the slurry was pasted on 1×1 cm^2 Ni foam by the use of a spatula. Then the electrodes were dried at 120 °C for 12 h. Full cell measurement was performed using $Co_3V_2O_8$ or Co_3O_4 as the cathode and AC as the anode, separated by a distance of 2 cm. Pt wire was used to connect the electrodes and the instrument. 3M KOH was used as the electrolyte. We have performed the asymmetric cell study in the voltage window of 1.6 V. To achieve the maximum specific capacitance value of the asymmetric cell, the storage capacity of negative and positive electrodes has to be balanced by the following equation,

$$1/C_{total} = 1/C_{cathode} + 1/C_{anode} \text{ ----------6}$$

Charge storage capacity of the asymmetric cell has been balanced by adjusting the mass ratio of $Co_3V_2O_8$ or Co_3O_4 and AC. Mass ratio was calculated by achieving the charge balance using the following equation,

$$m_+/m_- = (C_- \times \Delta E_-)/(C_+ \times \Delta E_+) \text{ ----------7}$$

where q_+, $q\_$, m_+, m_-, C_+, C_-, E_+, and E_- are the charge, mass, specific capacitance and potential windows obtained in the three-electrode measurement for the positive and negative electrode. For both asymmetric cell weight of the active material was 3 mg (for Co_3O_4//AC, Co_3O_4 : AC was 1 : 2 and for $Co_3V_2O_8$//AC, $Co_3V_2O_8$: AC was 1 : 7).

Figure S14 demonstrates the CV curve of $Co_3V_2O_8$//AC and Co_3O_4//AC at different scan rate. From the non rectangular CV curve in both the figure it can be concluded that capacitance in the asymmetric supercapacitor is dominated by the pseudocapacitance of the oxide materials compared to the double layer capacitance of the AC. Figure S15 illustrates the charge-discharge curve of the two asymmetric cell at different current densities. The highest specific capacitance of $Co_3V_2O_8$//AC and Co_3O_4//AC are 303 F/g and 121 F/g, respectively at 1 A/g current density. We also have checked the stability of the asymmetric supercapacitors up to 10000 cycles (Figure S16). According to the result,

$Co_3V_2O_8$//AC can retain 97% of its specific capacitance even after 10000 cycles where as for Co_3O_4//AC specific capacitance decreases to 74% after the same.

To characterize the superior electrochemical activity of the $Co_3V_2O_8$//AC over Co_3O_4//AC, we have performed the EIS measurement for both the cell. EIS measurements have been done within the frequency range from 0.1 Hz to 10^5 Hz at AC voltage amplitude of 5 mV. Figure S17a and b illustrate the Nyquist plot for $Co_3V_2O_8$//AC and Co_3O_4//AC, respectively. Figure S17a demonstrates that change in charge transfer resistance for Co_3O_4//AC asymmetric cell is very high, which may be due to the rupture of morphology of Co_3O_4 during the cycles at high current density. This is the reason behind the drastic change in the specific capacitance for Co_3O_4//AC after 10000 cycles. On the other hand, from Figure S17b, it can be observed that for $Co_3V_2O_8$//AC before and after 10000 cycles nature of the plot is almost same i.e, no such abrupt change in the internal resistance or charge transfer resistance has occurred. Thus $Co_3V_2O_8$//AC is considerably more stable after 10000 cycles. Figure S18 demonstrates the Ragone plot for the two asymmetric cells. The highest energy density for $Co_3V_2O_8$//AC and Co_3O_4//AC are 107 Wh kg^{-1} at power density 800 W kg-^{1} and 43.09 Wh kg^{-1} at power density 789.81 W kg^{-1}, respectively.

Tables:

Electrode Material	Specific capacitance	Type of electrode (current collector)	References
1. Co_3O_4@Pt@MnO_2	539 F/g at 1A/g	Three electrode cell (Ti foil)	S1
2. Co_3O_4 nanosheet	1782 F/g at 1.8 A/g	Three electrode cell (Ni foam)	S2
3. Co_3O_4	548 F/g at 8 A/g	Three electrode cell (Ni foil)	S3
4. Co_3O_4/rGO	402 F/g at 2 A/g	Three electrode cell (Ni foam)	S4
5. Co_3O_4/graphene	157.5 F/g at 0.1 A/g	Three electrode cell (Ni foam)	S5
6. $Co(OH)_2$ (alpha)	952 F/g at 5 mA/cm2	Three electrode cell (Ni foam)	S6
7. Co_3O_4@RuO_2	905 F/g at 1 A/g	Three electrode cell (carbon paper)	S7
8. $CoMoO_4$/graphene	2741 F/g at 1.43 A/g	Three electrode cell (Ni foam)	S8
9. $Co(OH)_2$ (beta)	2028 F/g at 1A/g	Three electrode cell (graphite)	S9
10. $Ni(OH)_2$	1677 F/g at 5 mV/S	Three electrode cell (graphite sheet)	S10
	153 F/g at 5 mV/S	Two electrode cell/asymmetric supercapacitor	
11. $Ni(OH)_2$	4172.5 F/g at 1A/g	Three electrode cell (Ni foam)	S11
12. Cl dopped carbonated $Co(OH)_2$	9893.75 F/g at 0.5 A/g	Three electrode cell (Ni foam)	S12
13. $NiCo_2O_4$	1450 F/g at 20A/g	Three electrode cell (Ni foam)	S13
14. $Co_3V_2O_8$	739 F/g at 0.5A/g	Three electrode cell (Ni foam)	S14
15. Co_3O_4 nanosheet $Co_3V_2O_8$ nanosheet	1256 F/g at 1A/g 4194 F/g at 1 A/g	Three electrode cell (no additional current collector), glassy carbon electrode	This work

Table S1: Specific capacitance of different reported electrode materials.

Current density (A/g)	Specific capacitance (C_1) (F/g)	Specific capacitance (C_2) (F/g)
1	1256	4194
2	1078	3877
3	1004	3566
4	946	3137
5	889	2911
6	837	2697
7	804	2537
8	788	2379
9	743	2191
10	7193	2080
11	705	1977
12	679	1820
13	659	1771
15	624	1733
20	566	1627
25	533	1515
30	461	1400

Table S2: Specific capacitance of C_1 and C_2 samples at different current densities.

Supercapacitor	Energy density value (Wh kg^{-1})	Reference
Symmetric supercapacitor		
$Ni(OH)_2$/carbon nanotube	50.6	S15
$Ni(OH)_2$	35.7	S10
β-$Co(OH)_2$	108.9	S9
$CoMoO_4$	37.25	S8
$CuCo_2O_4$	3.05	S16
$NiCo_2O_4$	22.6	S17
$Co3O_4$	62.8	This work
$Co_3V_2O_8$	209	

Table S3: Energy density of different reported supercapacitor.

		Internal resistance, R_S (ohm)	Charge transfer resistance, R_{CT} (ohm)	Diffusive resistance, W (ohm)
C_1	Initial	7.769	30.5	0.0027
	After 10000 Cycle	8.113	45.7	0.0098
C_2	Initial	6.78	17.48	0.0017
	After 10000 cycle	7.341	20.16	0.0033

Table S4: Parameters obtained from Nyquist plot for C_1 and C_2 samples before and after 10000 cycles.

References:

S1. . H. Xia, D. Zhu, Z. Luo, Y. Yu, X. Xhi, G. Yuan and J. Xie, *Sci. Rep.,* 2013*,* **3***,* 2978(1-8).

S2. Q. Yang, Z. Liu, X. Sun and J. Liu, *Sci. Rep.,* 2013*,* **3***,* 3537.

S3. . S. K. Meher and G. R. Rao, *J. Phys. Chem. C,* 2011, **115**, 15646.

S4. Z. Song, Y. Zhang, W. Liu, S. Zhang, G. Liu, H. Chen and J. Qui, *Electrochim Acta,* 2013, **112,** 120.

S5. Q. Guan, J. Cheng, B. Wang, W. Ni, G. Gu, X. Li, L. Huang, G. Yang and F. Nie, *ACS Appl. Mater. Interfaces,* 2014, **6**, 7626.

S6. Z. Gao, W. Yang, Y. Yan, J. Wang, J. Ma, X. Zhang, B. Xing and L. Liu, *Eur. J. Inorg. Chem.,* 2013, **27**, 4832.

S7. R. B. Rakhi, W. Chen, M. N. Hedhili, D. Cha and H. N. Alshareef, *ACS Appl. Mater. Interfaces,* 2014, **6**, 4196.

S8. X. Yu, B. Lu and Z. Xu, *Adv. Mater.,* 2014, **26**, 1044.

S9. S. Gao, Y. Sun, F. Lei, L. Liang, J. Liu, W. Bei, B. Pan and Y. Xie, *Angew. Chem. Int. Ed.,* 2014, **53**, 12789.

S10. H. B. Li, M. H. Yu, F. X. Wang, P. Liu, Y. Liang, J. Xiao, C. X. Wang, Y. X. Tong, G. W. Yang, *Nat. Commun.,* 2012*,* **4***,* 1894.

S11. Y. Zhu, C. Cao, S. Tao, W. Chu, Z. Wu and Y. Li, *Sci. Rep*., 2014, **4**, 5487.

S12. N. Mahmood, M. Tahir, A. mahmood, J. Zhu and C. Cao and Y. Hou, *Nano Energy,* 2015, **11**, 267.

S13. C. Yuan, J. Li, L. Hou, , X. Zhang, L. Shen and X. W. Lou, *Adv. Funct. Mater.* 2012*,* **22***, 4592.*

S14. Y. Zhang, Y. Liu, J. Chen, Q. Guo, T. Wang and H. Pang, *Sci. Rep*., 2014, **4**, 5687.

S15. Z. Tang, C. Tang, H. Gong, *Adv. Funct. Mater.,* 2012, **22**, 1272.

S16. A. Pendashteh, M. S. Rahmanifar, R. B. Kaner and M. F. Mousav, *Chem. Commun.*, 2014, **50**, 1972.

S17. H. Jiang, J. Ma and C. Li, *Chem. Commun.*, 2012, **48**, 4465.

Figures:

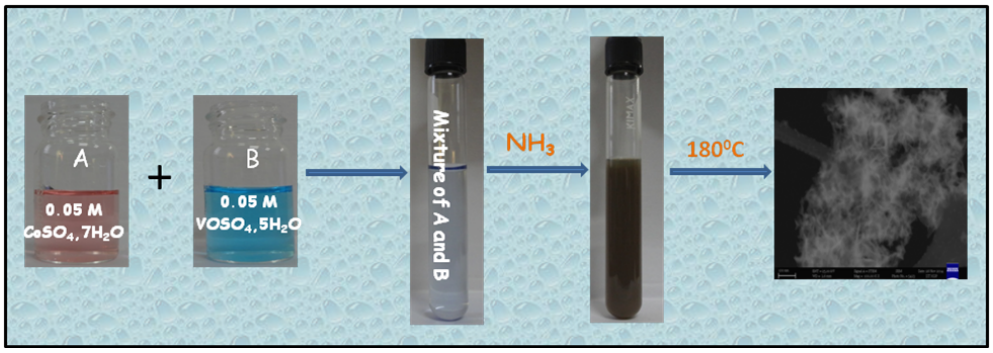

Figure S1: Schematic presentation of the synthesis of C_2 sample.

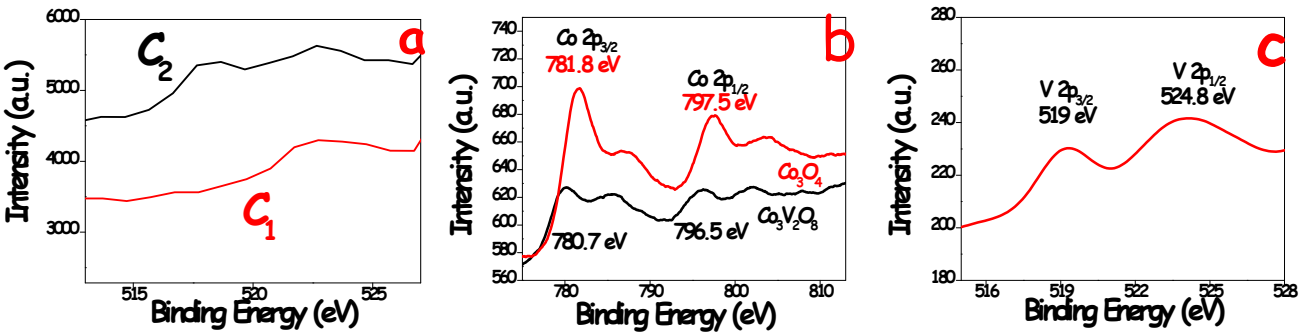

Figure S2: Narrow range XPS for a) C_1 and C_2 to indicate the presence of V in C_2, b) Co 2p and c) V 2p atom in C_1 and C_2 samples.

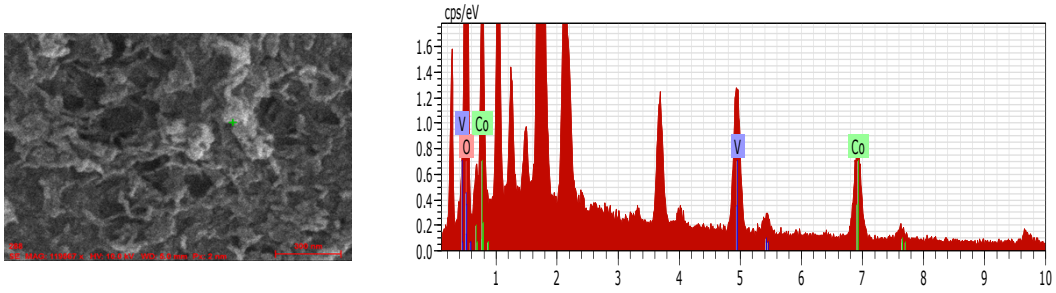

Figure S3: EDS profile of the C_2 sample.

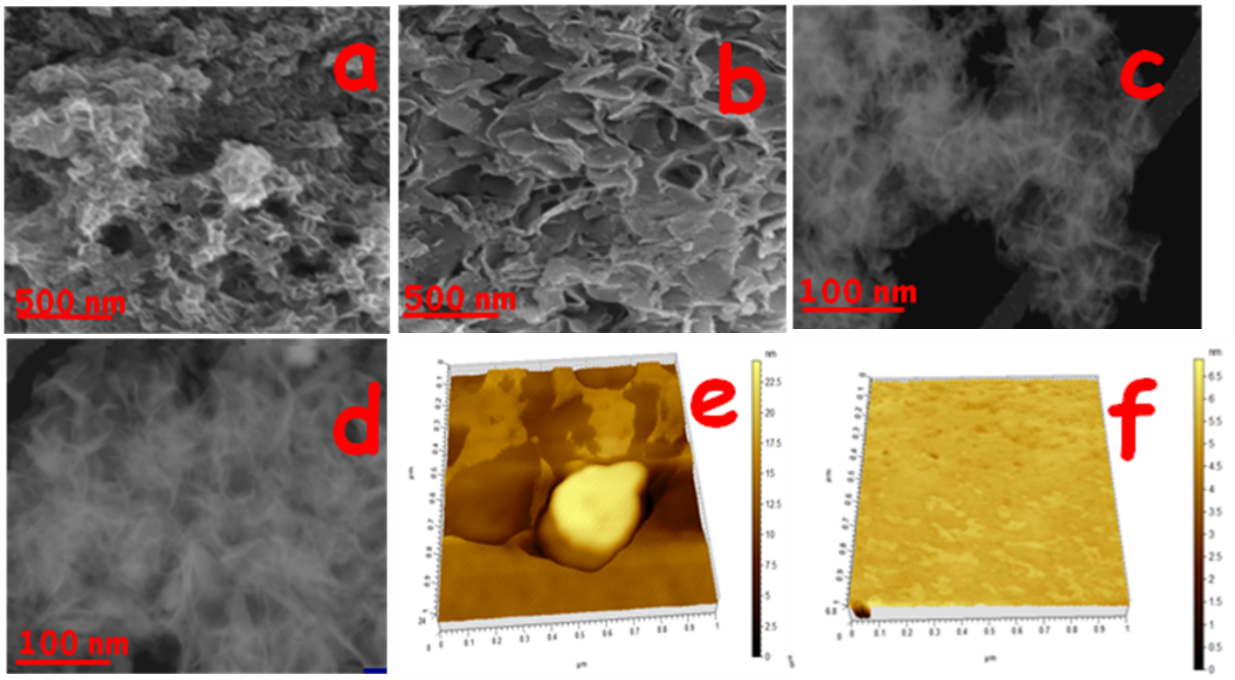

Figure S4: FESEM images of a) C_2 and b) C_1, STEM images of c) C_2 and d) C_1, AFM images of e) C_2 and f) C_1 samples.

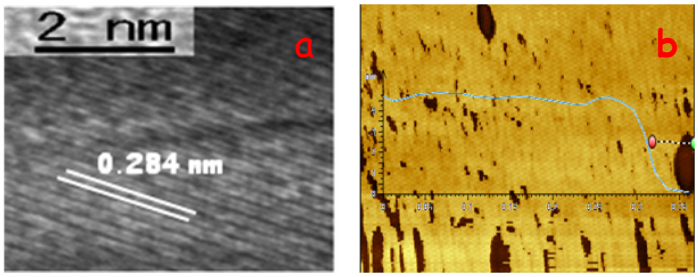

Figure S5: a) Fringe spacing and b) AFM thickness profile of C_1 sample.

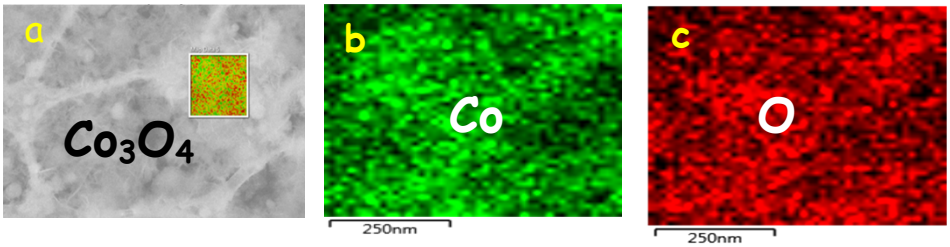

Figure S6. STEM image elemental area mapping of C_1 sample.

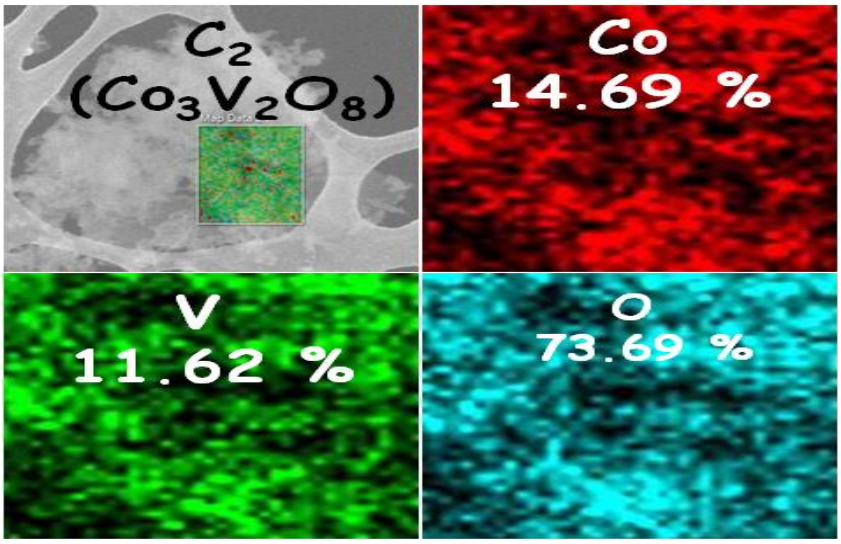

Figure S7: STEM image elemental area mapping of C_2 sample

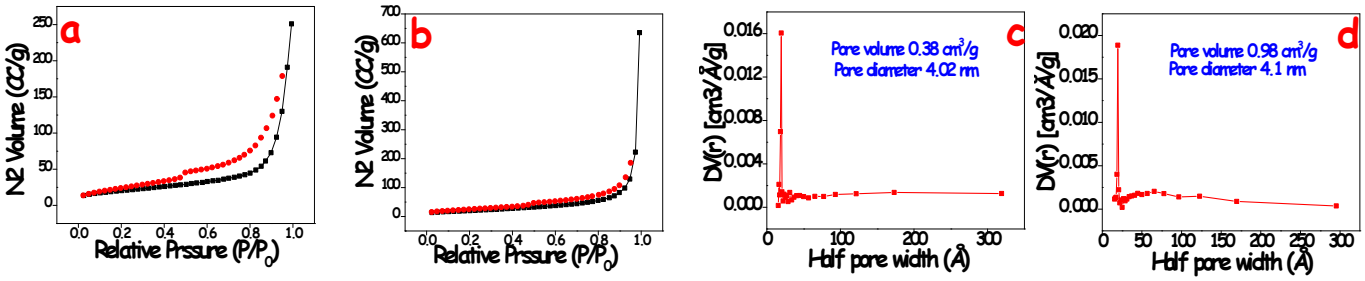

Figure S8: N_2 adsorption-desorption isotherm for (a) C_1 sample and (b) C_2 sample. Pore size distribution curve for (c) C_1 and (d) C_2 sample.

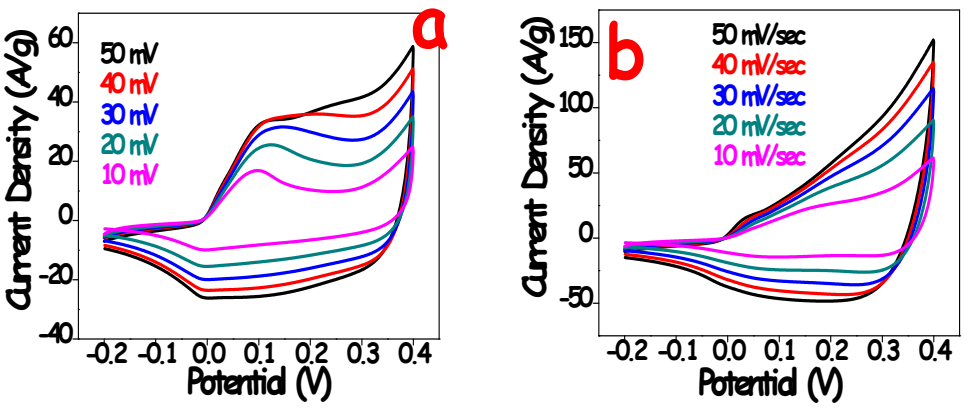

Figure S9: CV curves for a) C_1 and b) C_2 at different scan rates.

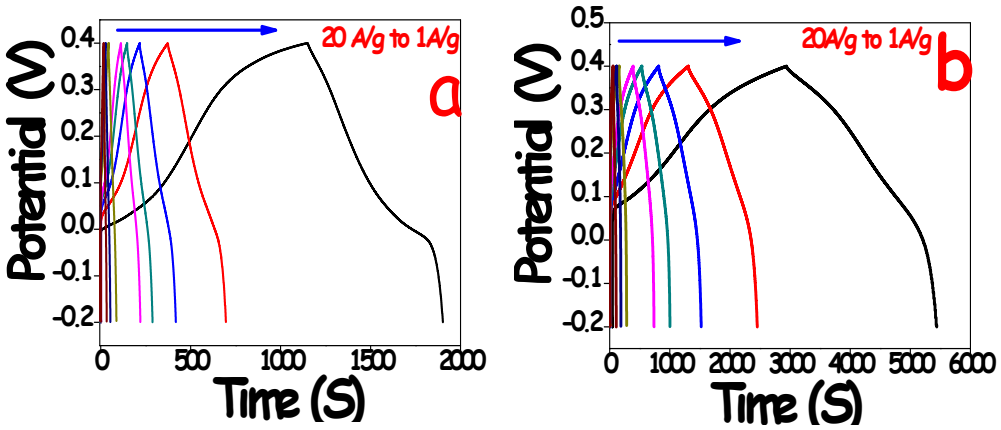

Figure S10: Charge-discharge curve of a) C_1 and b) C_2 at different current densities.

ISO 25178			
Height Parameters			a
Sq	0.992	nm	Root mean square height
Ssk	-2.81		Skewness
Sku	11.8		Kurtosis
Sp	2.25	nm	Maximum peak height
Sv	5.62	nm	Maximum pit height
Sz	7.87	nm	Maximum height
Sa	0.559	nm	Arithmetic mean height

ISO 25178			
Height Parameters			b
Sq	3.80	nm	Root mean square heigh
Ssk	0.676		Skewness
Sku	4.55		Kurtosis
Sp	11.1	nm	Maximum peak height
Sv	13.1	nm	Maximum pit height
Sz	24.3	nm	Maximum height
Sa	2.62	nm	Arithmetic mean height

Figure S11: Roughness profile of a) C_1 and b) C_2 obtained from AFM image.

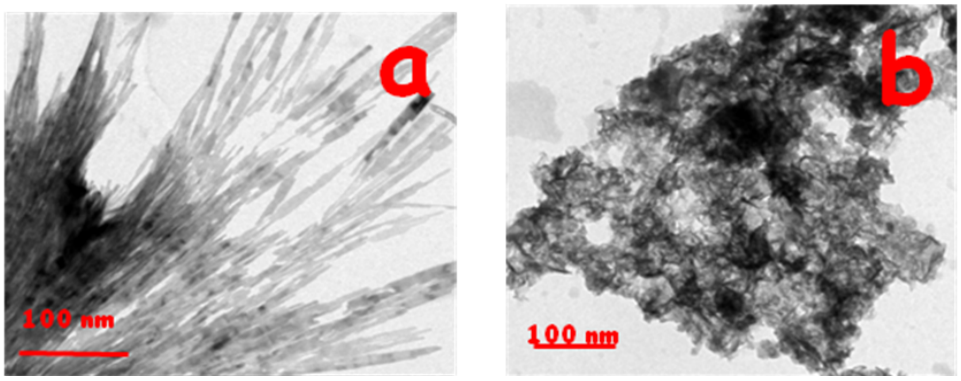

Figure S12: TEM images of a) C_1 and b) C_2 sample after 10000 charge-discharge cycle.

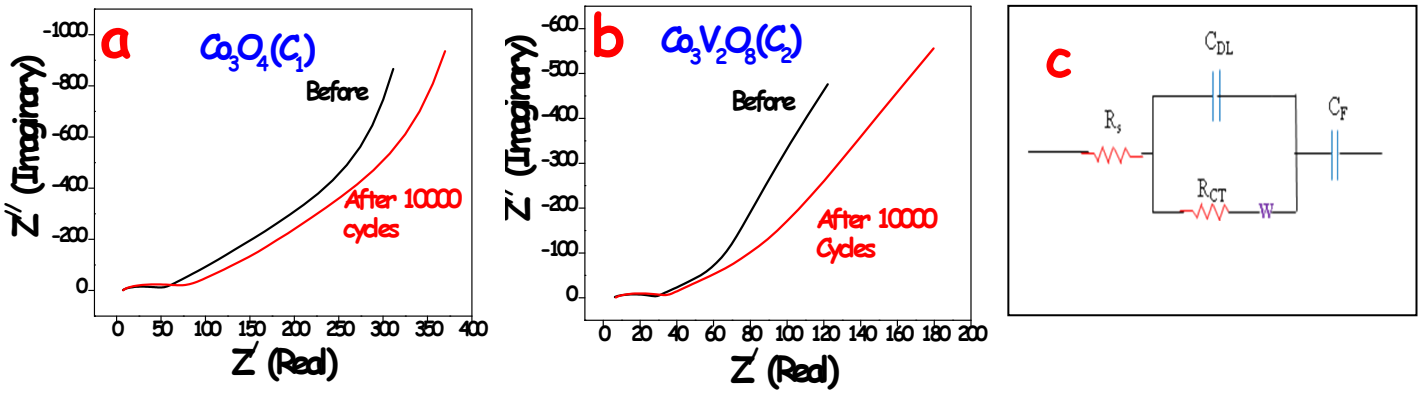

Figure S13: Nyquist plot for (a) C_1 and (b) C_2 samples before and after 10000 charge–discharge cycles, respectively. (c) The equivalent circuit of the supercapacitor, where C_{DL}, C_F , R_{CT}, R_S and W stand for double layer capacitance, pseudocapacitance, charge transfer resistance, internal resistance and Warburg constant, respectively.

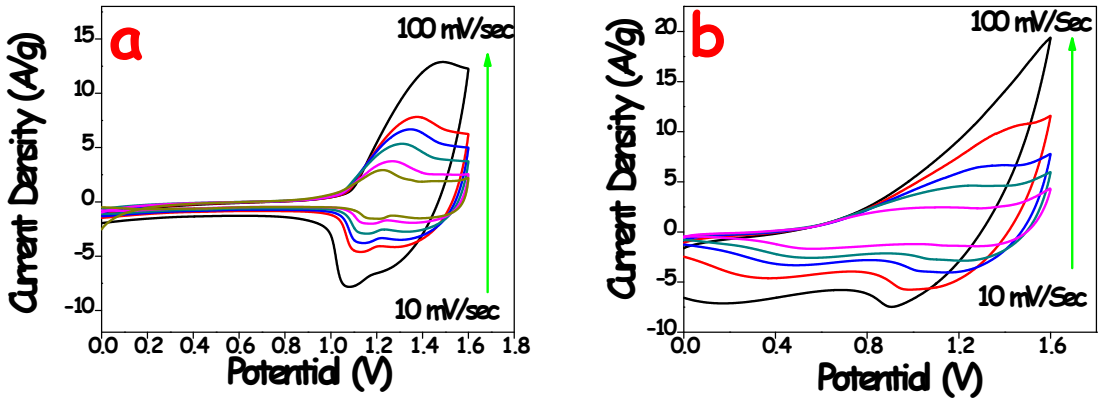

Figure S14: CV curve for (a) Co_3O_4//AC and (b) $Co_3V_2O_8$//AC at different scan rate.

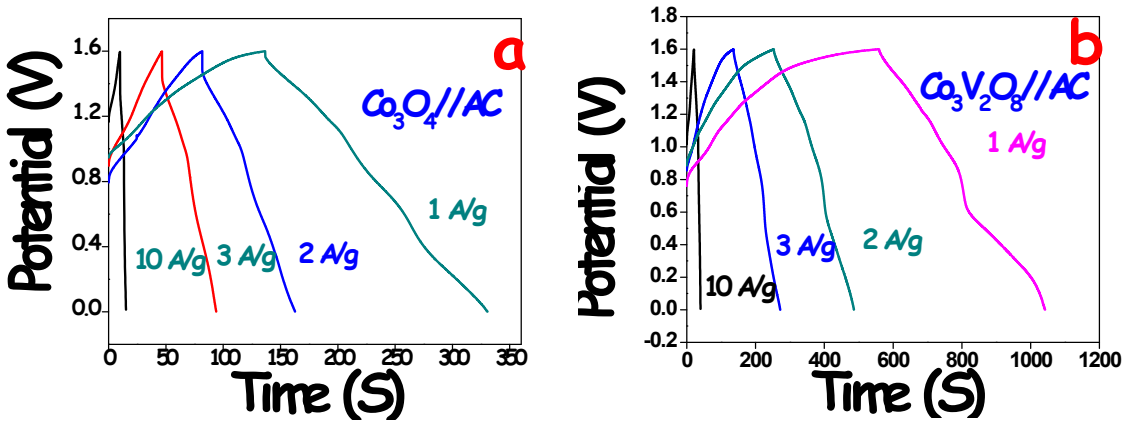

Figure S15: Charge-discharge curve for (a) Co_3O_4//AC and (b) $Co_3V_2O_8$//AC at different current densities.

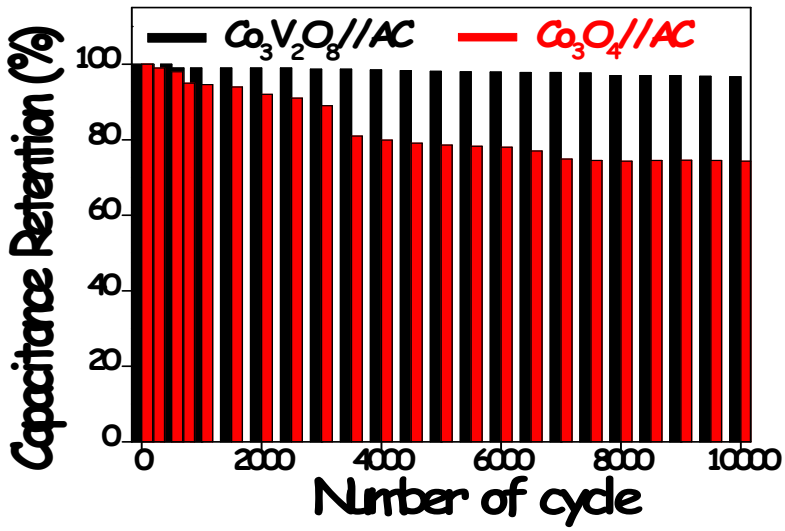

Figure S16: Comparative study of the percentage retention of specific capacitance for Co_3O_4//AC and $Co_3V_2O_8$//AC up to 10000 cycles.

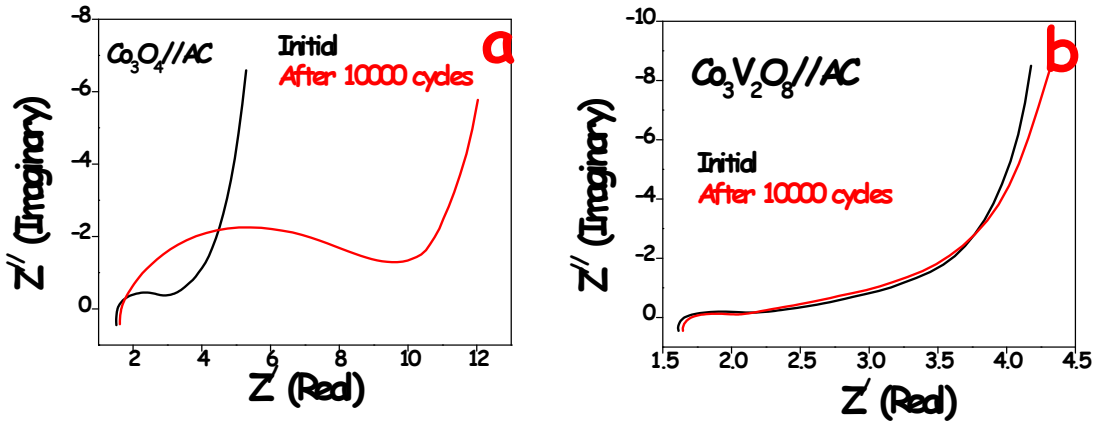

Figure S17: Nyquist plot for (a) Co_3O_4//AC and (b) $Co_3V_2O_8$//AC before and after 10000 cycles.

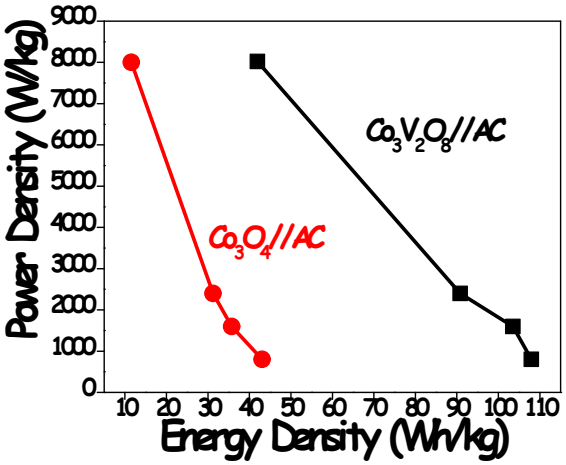

Figure S18: Ragone plot for Co_3O_4//AC and $Co_3V_2O_8$//AC.